JOURNAL OF GEOPHYSICAL RESEARCH, VOL. 98, NO. B10, PAGES 17,723–17,735, OCTOBER 10, 1993

Crustal Structure and Deep Reflector Properties: Wide Angle Shear and Compressional Wave Studies of the Midcrustal Surrency Bright Spot Beneath Southeastern Georgia

THOMAS L. PRATT,[1] JOEL F. MONDARY,[2] AND LARRY D. BROWN

Institute for the Study of the Continents, Cornell University, Ithaca, New York

NIKOLAS I. CHRISTENSEN

Department of Earth and Atmospheric Sciences, Purdue University, West Lafayette, Indiana

STEPHEN H. DANBOM

Conoco, Incorporated, Ponca City, Oklahoma

Three-component (*P*, *SH*, and *SV*) expanding spread profiles (ESP), common-midpoint profiles, and sparse three-dimensional *P* wave data were collected over an unusually strong midcrustal reflector, the Surrency Bright Spot (SBS), in southeastern Georgia. Shear wave reflections from the SBS at 10.9 s (16 km depth), and possibly from the lower crust at 18.3 s (29 km depth), were recorded but required substantial source effort (stacking) and were too weak for reliable reflectivity measurements. Reflections on the ESPs delineate a 1.5-km-thick Atlantic Coastal Plain section whose seismic properties (Vp=2.53 km/s, Vs=1.51 km/s, Vp/Vs=1.67) are consistent with quartz-rich sandstones and siltstones, sitting atop a 15-km-thick upper crust (Vp=6.38 km/s, Vs=3.25 km/s, Vp/Vs=1.96), which in turn overlies a 15 km-thick lower crust of slower material (Vp=6.02 km/s, Vs=3.26 km/s, Vp/Vs=1.84). The velocity inversion may result from underthrusting of upper crustal rocks during suturing of Florida to North America. Amplitude-versus-offset analyses, combined with an earlier reflection polarity test and waveform modeling, indicate that the SBS originates from a thin (~80-120 m), high-impedance layer, most likely a mafic dike or tectonically emplaced ultramafic body.

INTRODUCTION

One of the most unusual features imaged on Consortium for Continental Reflection Profiling (COCORP) data is the extremely reflective Surrency Bright Spot (SBS) located at 16 km depth beneath southeastern Georgia (Figures 1 and 2). The SBS is intriguing not only for its strong reflectivity but also because it is isolated in the midcrust and is flat and level for about half of its 4 km length on the original COCORP data (Figure 1).

The similarity between the SBS and fluid-related "bright spots" or "flat spots" seen on shallow seismic reflection data [*Backus and Chen*, 1975; *Ensley*, 1984] suggests that the SBS may be caused by fluids trapped within fracture porosity in the midcrust [*Brown et al.*, 1987; *Wille*, 1987]. The SBS lies within the inferred Alleghanian suture zone between Florida and North America [*Nelson et al.*, 1985*a*, *b*; *McBride and Nelson*, 1988; *Chowns and Williams*, 1983], and middle and lower crustal fluids could therefore come from subduction and/or metamorphism of relatively "wet" oceanic sedimentary rocks [e.g., *Fyfe*, 1986]. Fluids could also be released by dehydration from progressive metamorphism of middle and lower crustal rocks. Given that the pressure at SBS depths should be nearly 5 kbars, the pore spaces, presumably fracture porosity, must be kept open by high fluid pressure. The nature of fluids at that depth is also unknown, but presumably any fluid or gas would be supercritical.

Reanalysis of existing COCORP data [*Barnes and Reston*, 1992], as well as a test of the reflection polarity of the SBS [*Pratt et al.*, 1991], have cast doubt on the fluid hypothesis. *Barnes and Reston* [1992] reexamined the original COCORP profile and showed that the dipping southern portion of the reflection (Figure 1) is not a diffraction; after migration it is seen to originate from a sloping portion on the northern part of the reflector. In complementary papers to this one [*Mondary et al.*, 1991, 1993], the three-dimensional data over the SBS were analyzed; modeling the reflection shows that the SBS has a shape much like that of a 2.2-km-wide amphitheatre (Figure 3) with the flat portion (the stage) to the southwest. This concave upward shape suggests that the unusually large reflection amplitude may be due in part to reduced scattering of seismic waves because of a "buried-focus" geometry and, unlike the original anticlinal "trap" interpretation, provides no fundamental impetus for interpreting the SBS as originating from a fluid-filled porous zone. A key test for the fluid hypothesis is reflection polarity, but comparison of the SBS reflection with both a geophone polarity test and first break deflections indicates that the SBS produces an initial positive deflection and thus arises from a positive impedance contrast at depth. The polarity measurement contradicts a simple, fluid-filled porous zone model. Furthermore, *Barnes and Reston* [1992] and *Pratt et al.* [1991] conclude from waveform modeling that the SBS

[1]Now at Branch of Earthquake and Landslide Hazards, U.S. Geological Survey, Golden, Colorado.

[2]Now at Amoco Production Company, Houston, Texas.

Paper number 93JB01817.
0148-0227/93/93JB-01817$05.00

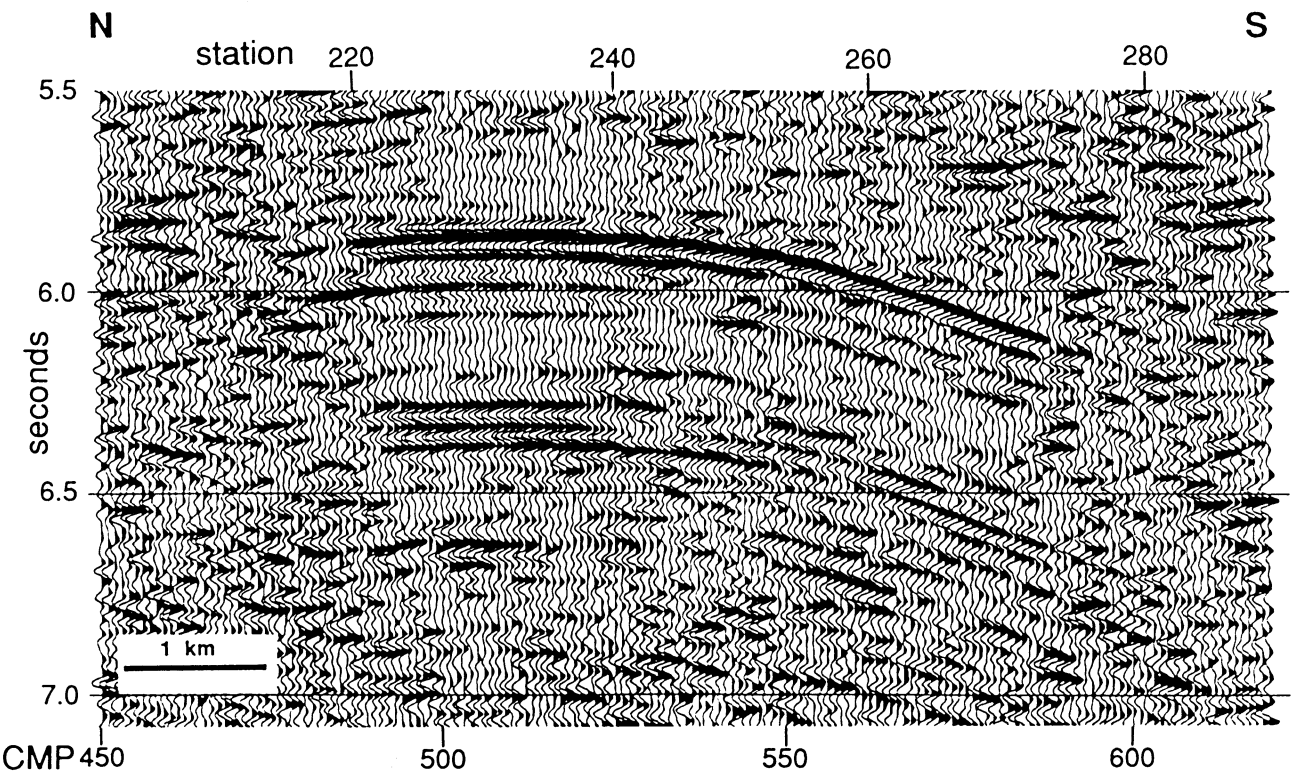

Fig. 1. The Surrency Bright Spot (SBS) as imaged on the original, unmigrated COCORP *P* wave common-midpoint (CMP) profile. See Figure 2 for location. Data are scaled with an automatic gain control and plotted with no vertical exaggeration assuming a crustal velocity of 6 km/s.

originates from at least two reflectors forming a thin (circa 80 to 150 m) layer. The only possible fluid model, therefore, must have two fluids with large, if not extreme, property contrasts to produce the strong "flat spot" reflector and a nonreflective top to the porous zone to prevent a negative reflection polarity.

This paper describes new seismic reflection data over the SBS acquired by COCORP in the summer of 1990. The new experiments consisted of compressional and shear wave common-midpoint (CMP) and expanding spread (ESP) profiles and the three-dimensional imaging of the SBS body. In addition to providing an accurate determination of the crustal velocity structure, the data have provided an effective test for evaluating our ability to determine material properties of deep reflectors and for assessing the feasibility of using shear wave vibrators for imaging middle and lower crustal features. Analysis of the new data for amplitude-versus-offset (AVO) characteristics, in conjunction with the previously measured positive reflection coefficient, indicates that the SBS indeed originates from a thin, high-impedance body.

Data Acquisition

The acquisition effort made use of a seismic group recorder (SGR) based, 600-channel, radio-controlled seismic system provided in part by Amoco Production Company. Geophones consisted of three-component, 10 Hz phones, six per string, deployed in 40-m linear arrays and aligned with a compass to keep the orientation the same as the vibrators. With both the vibrators and the phones, the *SV* mode refers to the in-line (or radial) sense of motion, and the *SH* mode refers to the transverse sense of motion.

Eight vibrators were used for sources, four smaller ones (40,000 lbs (178,000N) peak force) in *P* wave mode and four larger (52,000 lbs (231,000N) peak force *P* wave, 30,000 lbs (133,000N) peak force in *S* wave mode) used in *S* wave mode. The vibrators were deployed in a 40-m array (trucks were bumper-to-bumper), and vibration points (VPs) were spaced on average 1.2 km apart for a total of 32 VPs along the 37-km N-S line (Figure 2). Each VP consisted of an adjacent pair of source stations located 40 m apart, at each of which a 10-sweep *P* wave record was taken (20 sweeps/VP). *S* wave vibrators were swept 20 times at each station (40 sweeps/VP) with a new record after 10 sweeps. The sweep for all wave modes was a 20-s, 9-36 Hz upsweep. The pointed shear wave vibrator pads produced very small holes (10 cm or less in depth) in the hard portions of the packed-sand road (on which the VPs were preferentially sited) to holes about 0.5 m deep on soft portions. Because the SBS is located beneath remote timberlands, there was virtually no traffic (less than five vehicles per day), though logging operations caused a gap in one portion of the line.

Wide-angle reflections were recorded using a 130-station, three-component receiver array (390 channels total). Station spacing was 40 m to produce a 5.2-km spread length. A 48-s record length produced a 28-s correlated record, long enough to fully record any wide-angle reflections from Moho depths on the *S* wave records. The wide-angle reflection data are presented in two ways: as narrow, ~125-fold (*P*) and ~250-fold (*S*) common-midpoint (CMP) stacks (Figure 4) and as expanding spread profiles made from commmon-offset gathers (Figure 5). A second three-component array, 180 channels total, was kept adjacent to the vibrators, but the resulting common-

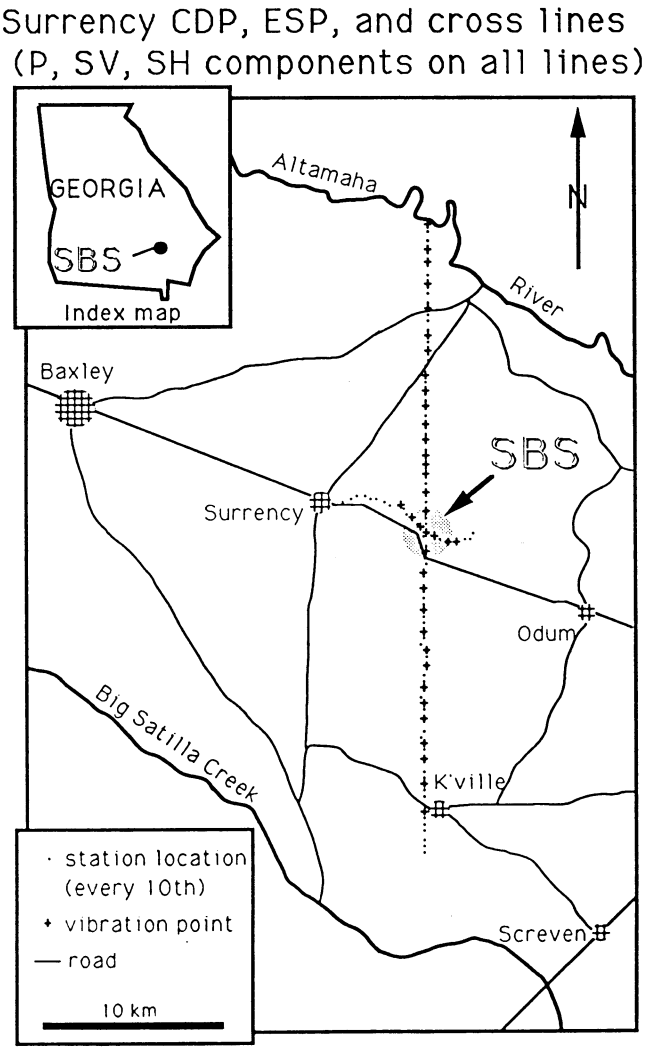

Fig. 2. Map of the southeastern Georgia region showing the location of the SBS and the seismic experiments conducted by COCORP in the summer of 1990. Dots show the location of every 10th receiver station, crosses show every source location. On the N-S profile both a CMP and an expanding-spread profile (ESP) were collected by using both wide angle and near-source recording arrays. The largest source-receiver offsets recorded in the ESP were 36.5 km.

midpoint sections are not shown here because the *P* wave data look like a noisy version of the original COCORP section (Figure 1) and the *S* wave sections show little energy below the Atlantic Coastal Plain (ACP) strata. To provide velocity and geometric control in the third dimension, a short (8.8 km) crossline was collected in each wave mode (Figure 2) and coarsely spaced, *P* wave three-dimensional data were acquired over a ~7 by 10 km grid. As mentioned above, forward seismic modeling of the three-dimensional data was used to determine an amphitheatre shape to the SBS [*Mondary et al.*, 1991, 1993].

CRUSTAL VELOCITY STRUCTURE

Reflection velocity analyses (Figure 4) can be used to define a three-layer crustal velocity structure (Figure 6) with layer boundaries at the base of the Atlantic Coastal Plain (ACP) strata, the Surrency Bright Spot (SBS), and the base of the crust. The isolated location of the SBS circumvents the reflector correlation uncertainties which normally plague comparative multicomponent velocity analyses. Both compressional and shear wave velocities, and thus Poisson's ratios, can be measured for the upper two layers, but determination of a shear velocity below the SBS is inaccurate.

Reflections at travel times of 1.92 s (*SH*) and 1.18 s (*P*) (Figure 4) are interpreted as originating from the top of crystalline basement rocks beneath the ACP strata. The stacking velocities are 1510 m/s and 2530 m/s, for a Vp/Vs ratio of 1.68 (Figure 6). The travel time ratio, on the other hand, gives a Vp/Vs ratio of 1.63 with the 3% discrepency most likely due to ray path distortion in the layered ACP strata [*Al-Chalabi*, 1973]. The measured velocities are typical for relatively quartz-rich sedimentary rocks like the sandstones and siltstones making up the ACP strata. The thickness of the Cretaceous and younger ACP strata, about 1.47 km, is in good agreement with drill holes in the region (the nearest is about 20 km away) which show pre-Cretaceous volcanic rocks at 1.3 km depth [*Chowns and Williams*, 1983].

From the expanding spread profiles in each wave mode (Figure 5), refracted arrivals can be used to define a two-layer velocity model within the ACP strata. The first layer is only about 300 m in thickness, with relatively low velocities of 1970 m/s (*P*) and 1060 m/s (*SH*) (Vp/Vs ratio of 1.86), and probably corresponds to the unconsolidated sands and silts at the top of the ACP section. The second layer is about 1.4 km in thickness, has velocities (3550 m/s *P*, 1870 m/s *SH*; Vp/Vs ratio of 1.9) typical of sedimentary rocks, and likely represents the bulk of the Atlantic Coastal Plain marine sedimentary strata. The fastest arrivals on the refraction data have velocities (5910 m/s *P*, 3620 m/s *SH*; Vp/Vs ratio of 1.6) representative of crystalline rocks; they are interpreted to be from widespread felsic volcanic layers forming the top of pre-Cretaceous basement [e.g., *Chowns and Williams*, 1983]. The 1.86 and 1.9 Vp/Vs refraction velocity ratios contrast with the 1.63 reflection velocity ratio and, as with the discrepency in the thickness of the ACP strata (1.7 km refraction, 1.47 km reflection), probably results from the refracted waves sampling specific layers and the reflected energy sampling all the strata.

The SBS is prominent on the *P* wave stacked sections at 5.9 s and easily visible on the *SH* wave section at a travel time of

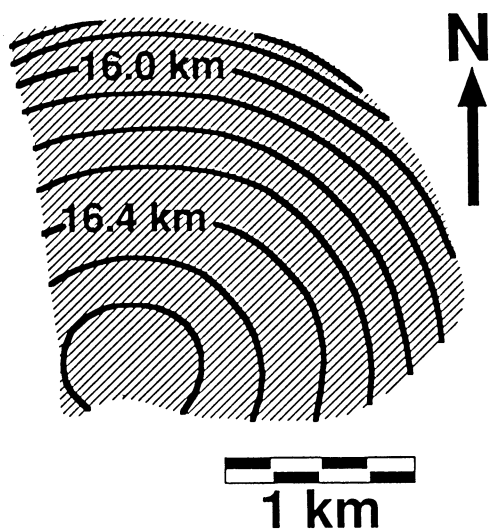

Fig. 3. Contour map of the SBS reflector as determined from modeling of the three-dimensional data. The feature is about 2.2 km in diameter and is shaped much like an amphitheatre, with the stage to the southwest.

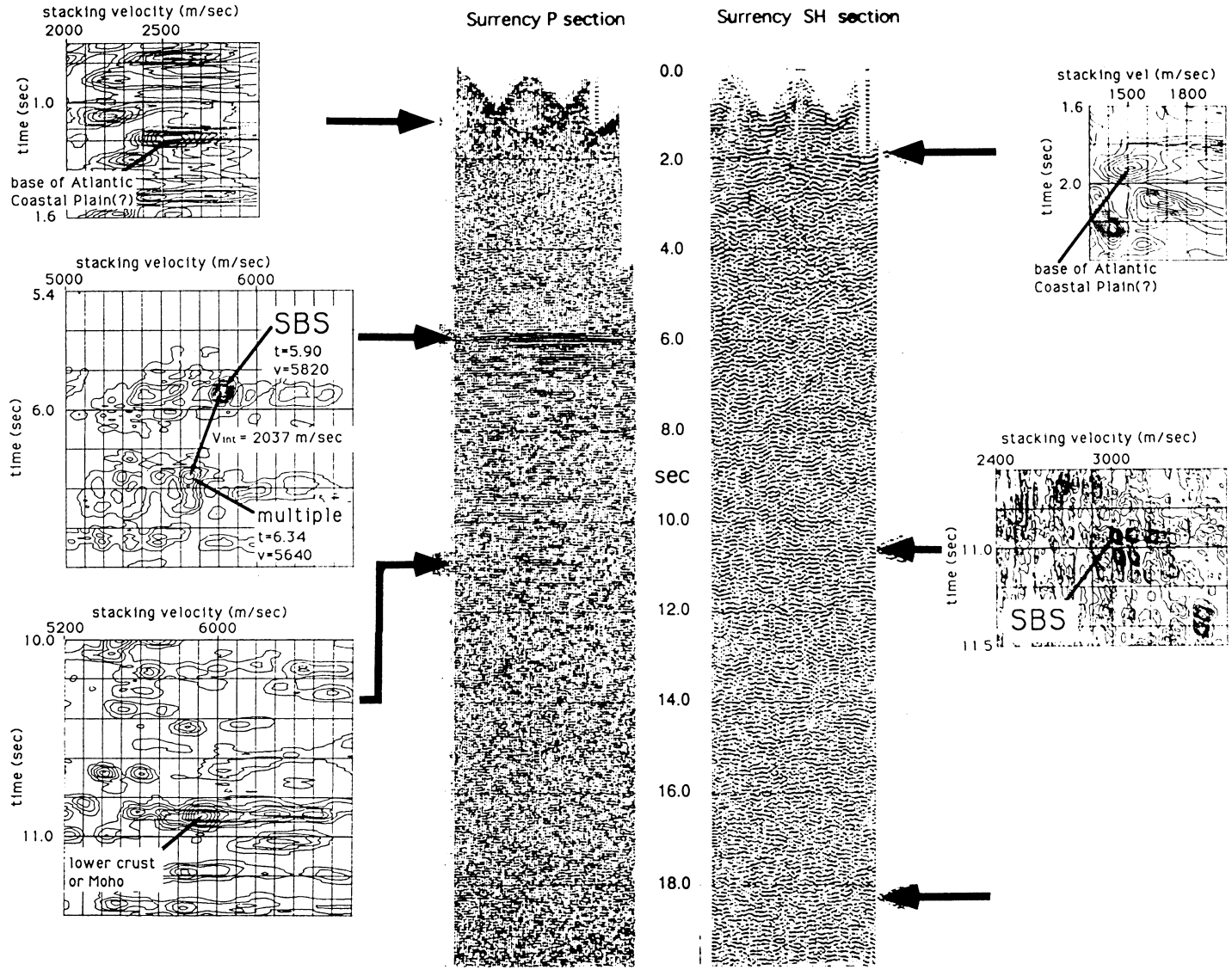

Fig. 4. *P* and *SH* wave stacked sections made from the wide-angle data, and the corresponding velocity analyses [*Taner and Koehler*, 1969] for the major reflectors. These stacked sections have a width of only 2.6 km (one half receiver spread). The sections are horizontally exaggerated in the plot (*P*~4.5:1 at 6 km/s; *SH*~9:1 at 3 km/s). Arrows and velocity analyses are for reflections at the base of the ACP strata, the SBS, and the lower crust. Both sections have been slightly coherency enhanced [e.g., *Robinson and Treitel*, 1980].

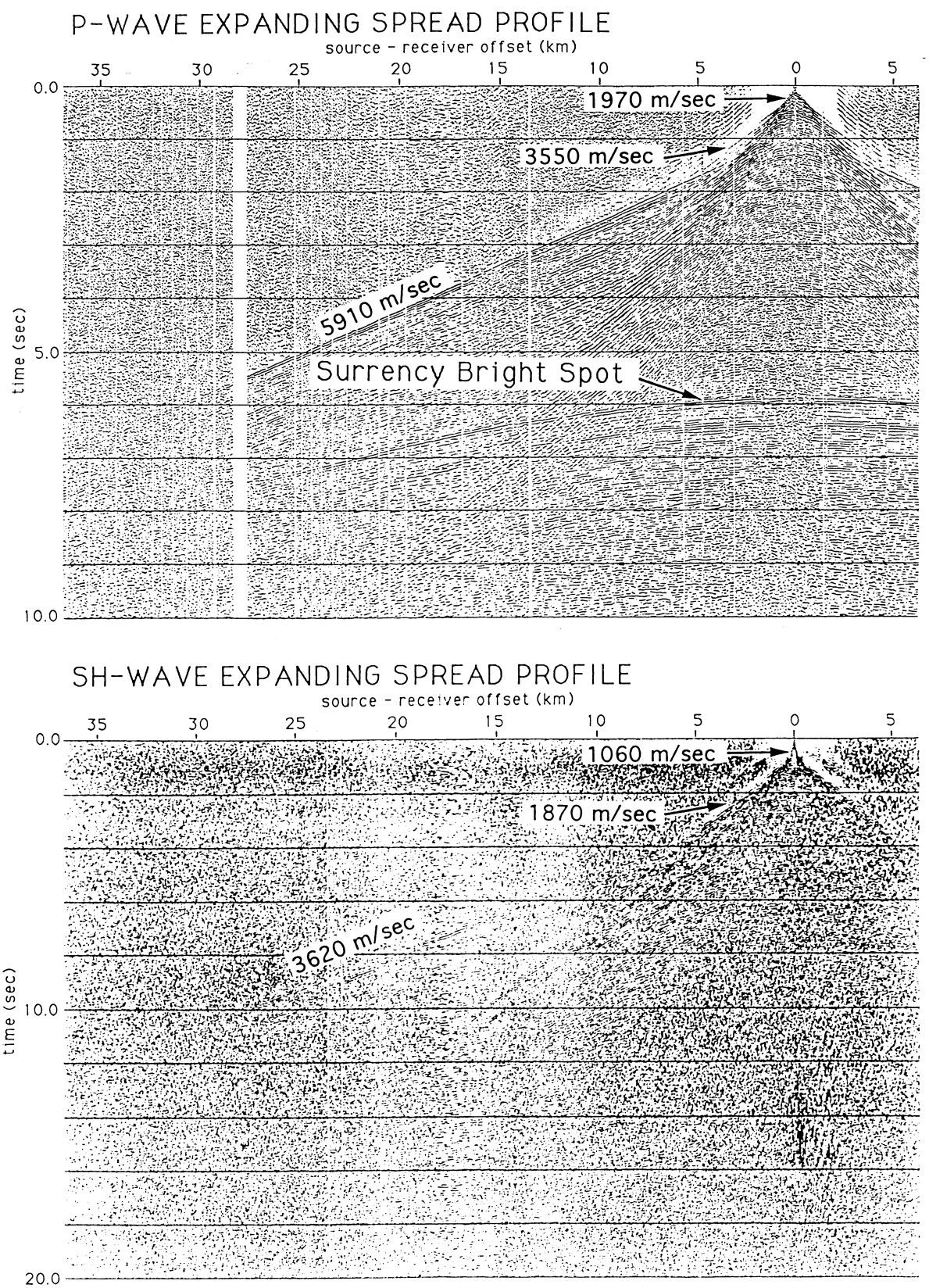

Fig. 5. *P* and *SH* wave ESPs collected over the SBS to offsets of up to 36.5 km, processed and displayed as common-offset gathers (only one side of the gather is fully displayed). The leftmost traces correspond to having the vibrators at the north end of the line and the receivers at the south. Numbers on the sections are the refraction velocities computed for each of the arrivals shown. *SV* wave data, not displayed here, contain both *P* and *S* arrivals and therefore look like a (noisier) combination of both of these profiles.

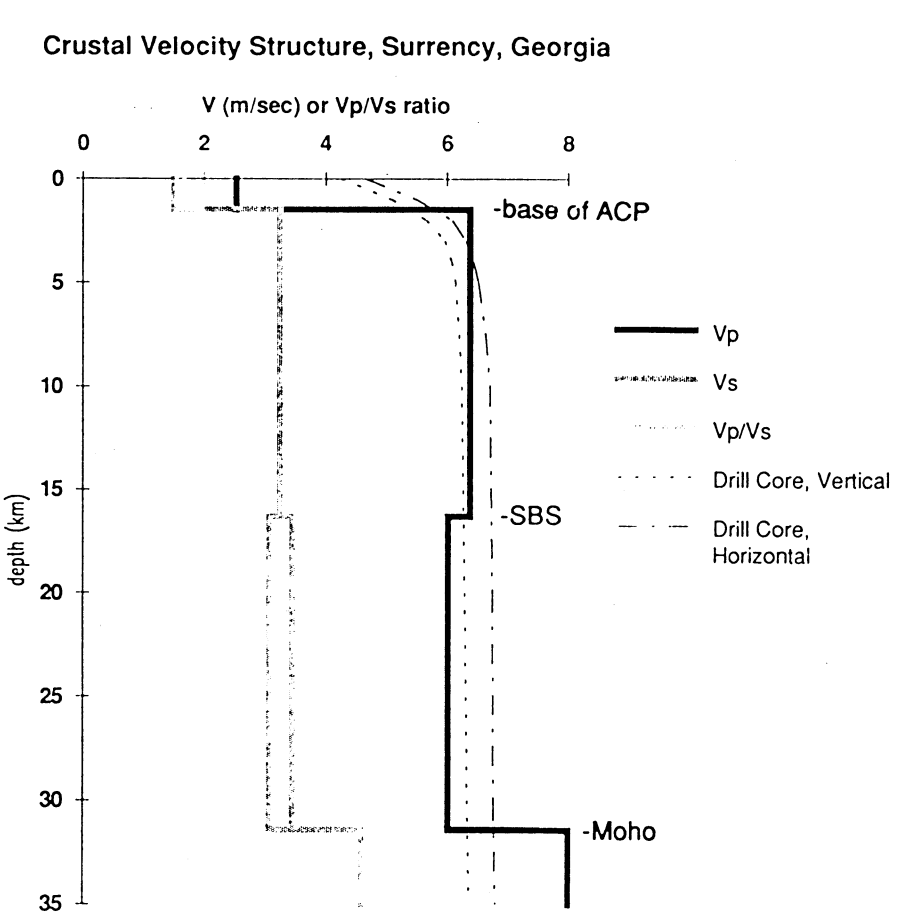

Fig. 6. Interval velocities computed from the reflection data using the Dix equation [e.g. *Dobrin*, 1976]. Note the decrease in Vp and possibly Vp/Vs in the lower crust. The upper 1.5 km are the relatively low-velocity Atlantic Coastal Plain (ACP) strata; the SBS lies in the midcrust and allows for independently measuring the bulk velocities in the upper and lower crust. Mantle velocities are from *Taylor* [1989]. The shear wave velocity (Vs) and Vp/Vs ratio in the lower crust have two values representing extremes of the estimated error (see text). The drill core data are from *Christensen* [1989].

10.9 s (Figure 4). Stacking velocities are 5820 m/s (*P*) and 3020 m/s (*SH*) with interval velocities between the ACP strata and the SBS reflector of 6380 and 3250 m/s. The bulk Vp/Vs ratio is 1.96 (Figure 6) whereas the travel time ratio is 1.91 (about 3% lower) for the same interval. Modeling to assess the effects of ray path bending indicate that the *P* wave stacking velocity is within about 2% (130 m/s) of the correct value, but secondary semblance peaks at 3100 and 3270 m/s on the *S* wave semblance computations (Figure 4), probably caused by trace-to-trace miscorrelation of the wavelets, suggest a 3% uncertainty in the *S* wave velocity determination.

The upper crustal shear velocity of about 3250 m/s is about 150 to 250 m/s, or about 5% to 8%, smaller than would be expected given the 3400 to 3500 m/s upper crustal shear velocity measurements determined in other studies in the southeastern United States (summary given by *Taylor* [1989]). The shear velocities measured here are vertical determinations, whereas the horizontally traveling waves used in the earlier teleseismic and surface wave studies may show higher velocities because of anisotropy [e.g., *Christensen*, 1989] and layering.

A strong lower crustal or Moho reflection is seen on the *P* wave data at 10.9 s with a stacking velocity of 5910 m/s; the *P* wave interval velocity of 6020 m/s between the SBS and this lower reflector is about 6% slower than the upper crustal velocity of 6380 m/s. This is a much larger discrepancy than the 3% errors in the velocities indicated by modeling and thus appears to be a real velocity inversion. The SBS lies at the top of a zone of reflectors which dip to the south (Figure 4; note that this section is horizontally exaggerated so the dips are not apparent) and which have been interpreted as a crustal shear zone related to the Late Paleozoic suturing of Florida to North America [*Nelson et al.*, 1985a]. The crustal velocities just described support this hypothesis if substantial amounts of relatively low-velocity material such as underthrust (meta)sedimentary strata are present.

One of the most tantalizing aspects of the data is an apparent arrival at 18.3 s travel time on the *SH* stacked section (Figure 4), which may correspond to one of the 9.6- to 10.0-s *P* wave reflections and would be one of the deepest shear wave reflections recorded from a vibrator source. Though a tremendous source effort was used (this is a 250-fold section), this result suggests that shear wave vibrators may be useful for limited deep-crustal work under the right conditions. This study used a shear-wave effort about 4 times that of the *P* wave, as measured in vibration time, but the need for an even greater effort is indicated by these results.

The *SH* wave reflection at 18.3 s stacks at a velocity of 3120 m/s, but this velocity is poorly constrained. An interval velocity below the SBS of 3262 m/s and a Vp/Vs ratio for the lower crust of 1.84 results; we cannot get a Vp/Vs travel time ratio because the corresponding *P* wave reflection cannot be identified. It is difficult to assess the error in this measurement, but a 6% error

(+/- 300 m/s) would produce interval velocities in the 3065 to 3460 m/s range or Vp/Vs ratios in the 1.96 to 1.73 range (Figure 6). The Vp/Vs ratio may thus drop in the lower crust relative to the upper crust, but the estimated errors allow for no Vp/Vs change as well.

Crustal refraction experiments generally show lower crustal *P* wave velocities in the 6500 to 6800 m/s range in the eastern United States [*Taylor*, 1989], and recent work on the South Carolina coastal plain [*Madabhushi et al.*, 1991; W. Mooney, personal communication, 1992] shows lower crustal velocities of 6400 to 6600 m/s. We interpret the relatively low crustal velocities obtained in the SBS reflection experiment (6020 and 6380 m/s) as due in part to anisotropy, with the vertical velocities about 6% to 10% lower than horizontal velocities. Although the nearest laboratory measurements were made on rocks nearly 350 km to the northwest [*Christensen*, 1989], the Inner Piedmont rocks there also showed a 6% lower horizontal velocity (Figure 6). The origin of this latter anisotropy is preferred mineral orientation of mica and amphibole in the metamorphic rocks. In addition, velocity differences can also occur because the refracted energy travels along the fastest layers, whereas the reflected energy time averages all of the layers.

A prominent reflection whose origin has been a subject of debate with the earlier COCORP data occurs 0.44 s below the SBS on the *P* wave stacked sections (Figure 1). The interval velocity of 2040 m/s determined here (Figure 4) strongly suggests that the second arrival is multiply reflected within the ACP sedimentary rocks. The alternative explanation is a ~450-m-thick, low-velocity (2040 m/s) zone, but if a fluid (water) is trapped within 6000-m/s crystalline rock, the time average equation [*Wyllie et al.*, 1956, 1958] predicts that an unreasonably high porosity of 39% is required. Furthermore, the impedance increase at the SBS interface [*Pratt et al.*, 1991] argues against a thick porous zone.

AMPLITUDE-VERSUS-OFFSET (AVO) ANALYSIS

The *P* wave data were analyzed to determine the reflection amplitude at differing offsets or incidence angles. Traces going into the analysis had no processing beyond a CMP sort and normal moveout correction; in particular, no amplitude corrections were applied. *S* wave data were not used because the SBS reflection was not visible at a sufficient range of offsets; it is unclear, however, whether the weakness of the *S* wave event is the result of a weak reflector or merely a lack of signal penetration, so we cannot use this information to constrain the interpretation.

An important issue in AVO analyses is which amplitude to measure. Interference between reflections from the top and bottom of the thin bed SBS, each of which may have a different AVO response, could complicate the AVO analysis. Figure 7 shows a comparison of normalized absolute values of different portions (both positive and negative offsets) of the reflected wavelet taken from common-offset stacks (1-km windows). Note that the three first lobes of the wavelet and the peak of the envelope function show a broadly similar pattern of decay with increasing offset. The median values (0.5-km offset windows) of the largest peak and largest trough of the SBS wavelet (effectively the first peak and first trough) also show an almost identical signature. We thus conclude that the AVO response is similar for the major lobes of the SBS wavelet. We will use the AVO response of the maximum amplitude of the SBS reflector in the subsequent analysis; this corresponds with the first peak of the wavelet and should minimize the interference from later arrivals (i.e., the bottom of a thin bed).

A distinct asymmetry is apparent on the AVO plot (Figure 8), with a higher initial amplitude but greater decay when sources are to the north (negative source-receiver offset values). This asymmetry is likely a combination of two effects. First, the three-dimensional study indicates that the SBS is amphitheatre shaped, and two-dimensional finite-difference modeling of the SBS indicates that the curved shape of the SBS creates larger reflection amplitudes when the source is to the north (Figure 9). Second, the road for several kilometers south of the SBS was very soft as it traversed a swampy area, and the AVO response shows a relatively weak signal when the vibrators are immediately south of the SBS (0 to +10 km on Figure 8). To the north of the SBS, however, the roads were quite hard, and the corresponding records (0 to -5 km on Figure 8) show a strong reflection. In our first look at AVO we ignore the asymmetry by looking at the absolute value of offset.

The AVO characteristics (Figure 10) are a function of the following: (1) spherical divergence; (2) reflector shape and size (a smaller percentage of the Fresnel zone is being reflected at larger offsets); (3) overburden effects (including source-receiver coupling); (4) anelastic attenuation; and (5) the AVO characteristics of the reflector (material properties).

Of these, the spherical divergence, reflector size, and anelastic attenuation can be estimated; Figure 11 shows the relative effects for each of these factors. Spherical divergence, which can be accurately computed [e.g., *Dobrin*, 1976], produces an amplitude drop of about 25% across our 40-km offset range.

The SBS size is a factor because less of the energy is being returned from the relatively small SBS reflector as the Fresnel zone increases in size and greater incidence angles reduce the

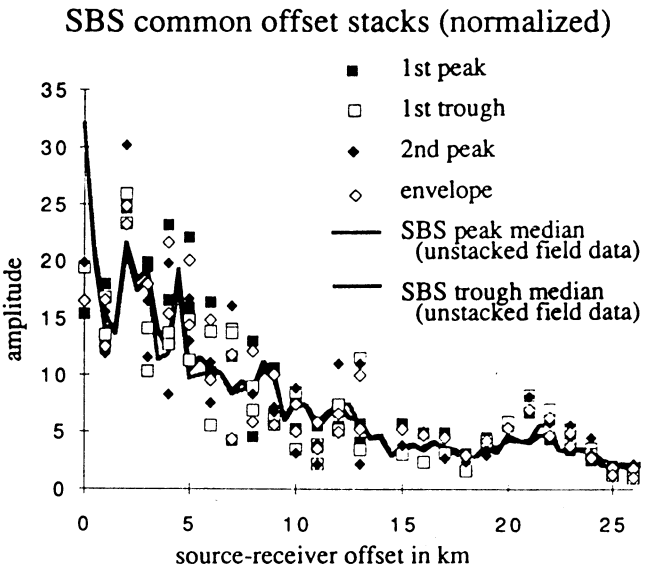

Fig. 7. Comparison of amplitudes versus source-receiver offset (absolute value) for several measures of the SBS reflected wavelet. Note that all of the measures produce a broadly similar response, but particularly note that the median values of the largest (first) peak and largest (first) trough are nearly identical. This graph suggests that the major lobes of the SBS reflection wavelet have essentially the same AVO response.

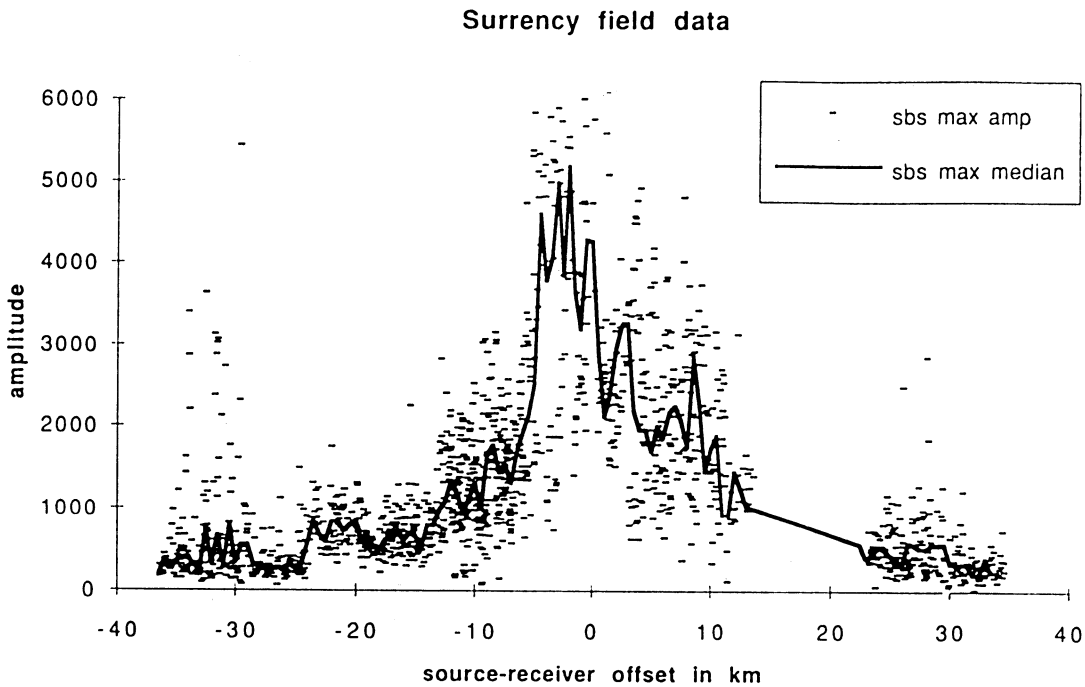

Fig. 8. Amplitude versus source-receiver offset for the maximum amplitude (first peak) of the SBS reflection wavelet. Each point represents a trace, the line represents the median of all traces within a 0.5-km offset range. For clarity, only one third of the single trace values are plotted. Positive offsets correspond to having the sources to the south and receivers to the north. Note the asymmetry of the response. The data between 12 and 23 km were edited because of high noise levels created by logging operations.

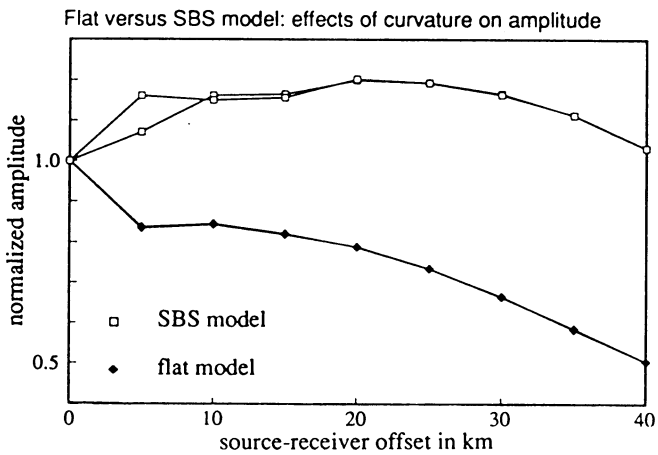

Fig. 9. Finite difference, acoustic, two-dimensional modeling assessing the effects of reflector shape on the AVO response of the SBS. The solid symbols show the response of a flat body with the same width, thickness, and material properties as the SBS model. The source and receiver were reversed during the modeling to produce two lines for each model, but in the flat model these lines are coincident. The SBS model shows an amplitude peak at 20 km offset due to focussing, with a lower amplitude at zero offset due to sideways scattering from the sloped body. The SBS response is asymmetric, with slightly larger amplitudes at the near offsets when the sources are to the north, as is observed in the field data (Figure 8).

effective SBS size due to oblique imaging at larger offsets. This effect can be estimated by assuming the SBS is a circular feature 2.2 km in diameter and then computing the percentage of the Fresnel zone reflected at each offset. This calculation simply consists of computing the area of the Fresnel zone and the apparent area of the SBS (taking the incidence angle into account) to determine the percentage of energy reflected from the SBS; the square root gives us the amplitude. Figure 11 shows that this effect reduces amplitudes by about 10% at the larger offsets.

Reflector shape can effect the reflection amplitudes by focussing and defocussing the energy at different points. Figure 9 compares responses from two-dimensional, finite difference, wave equation acoustic modeling of the curved SBS and a flat feature with the same width, thickness, and material properties. The source and receiver in the modeling were reversed to examine the reciprocity, but the two lines for the flat model coincide. As expected, the flat model produces a significant drop in amplitude at larger offsets. The SBS model, in contrast, shows a low amplitude near-zero offset because of scattering by the tilted SBS reflector and an amplitude peak (focussing) near the 20 km source-receiver offset. From this modeling we conclude that the reflector shape has an effect opposite to the trend observed in the field data, thus the ampliude decrease at greater offsets (Figure 10) would be even more pronounced if not for the curvature of the SBS reflector. We will ignore this effect during the rest of this analysis.

The effects of surface variability and coupling are difficult to assess, but the high multiplicity of measurements and the flat-lying near-surface strata should reduce short wavelength components. Unfortunately, standard source-receiver amplitude corrections [*Taner and Koehler*, 1981] could not be calculated because the unusual acquisition geometry and the lone reflection (the SBS) would cause any such corrections to also remove the desired AVO effects. However, the large multiplicity of the data (circa 4800 traces to define the observed AVO curve) and the reversal of the experiment allow us, by taking the median values at each offset, to include six to eight shot and receiver locations at each offset. This should reduce the effects of small

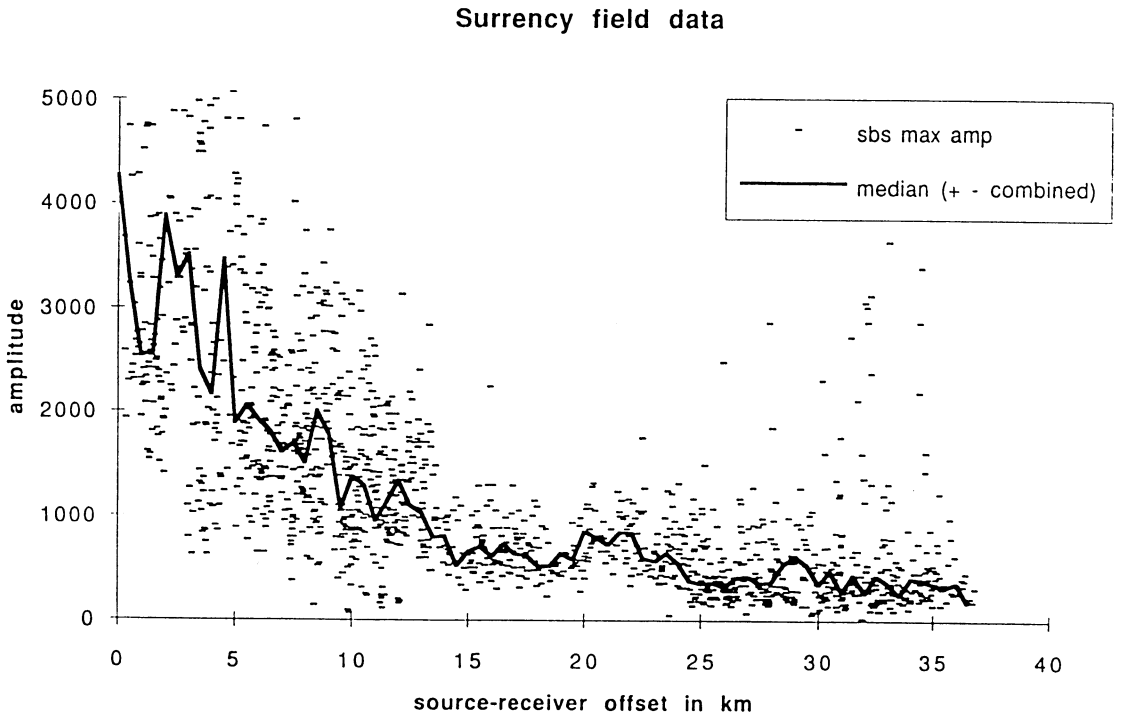

Fig. 10. Amplitude versus source-receiver offset (absolute value) for the Surrency field data. Dots represent individual traces, the line represents the median of all traces within 0.5-km offset ranges. For clarity, only one third of the traces are plotted.

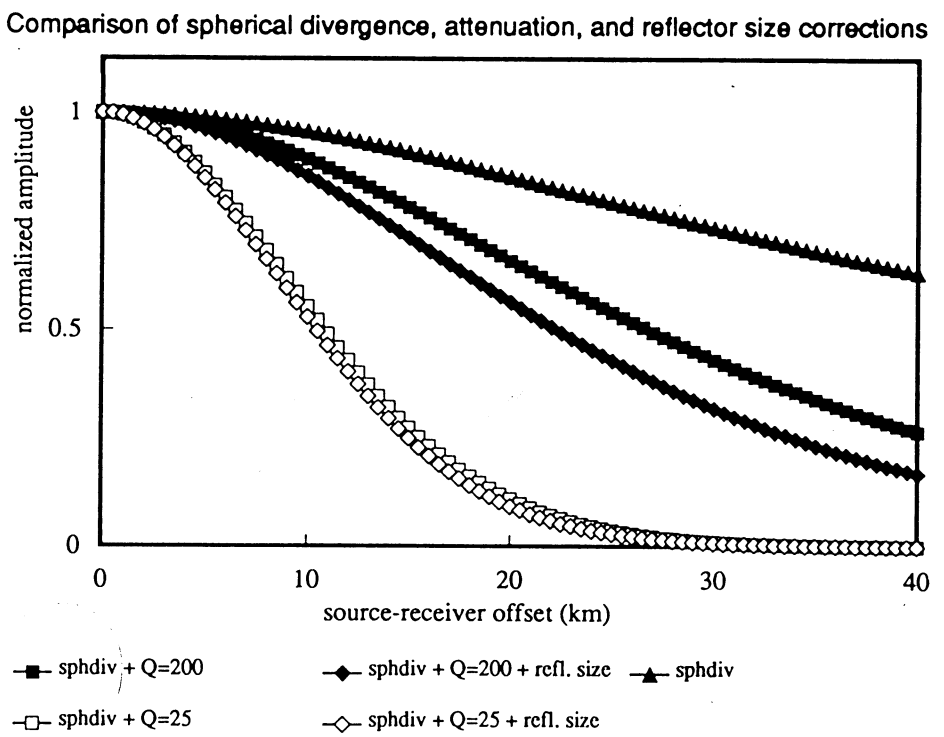

Fig. 11. Graph of amplitude versus offset response showing the relative effects of spherical divergence (sphdiv), anelastic attenuation (Q=25 and 200) and reflector size (refl. size) on the SBS reflection amplitude. If none of these effects were present, the model response in this figure would be flat with a value of 1.0. The reflector size takes into account the ratio of the SBS reflector area versus the Fresnel zone area, including changing incidence angle.

numbers of anomalous shot or receiver locations. Taking a running average of these median values over a 4-km window (Figures 12-14) further averages the near-surface effects. In addition, it must be kept in mind that the near-surface rocks consist of flat-lying ACP strata which show relatively little lateral change over the distance of the experiment.

Attenuation effects are difficult to separate from AVO effects, but for reasonable values of attenuation (Q>50) there is clearly a decrease in reflection amplitude with increasing offset. Figure 12 should reveal the AVO effects caused by the material properties by correcting for spherical divergence, reflector size, and different levels of anelastic attenuation [e.g., *Dobrin* 1976]. Looking only at the data at less than 25 km offset (at which point the relatively high noise levels at the ends of the profile make the results questionable (see Figure 5)), it is apparent that a value of 25 for Q is far too low because we do not expect the reflection to have an amplitude 4 times that at zero offset even under remarkable conditions (critical angles should not be reached until about 40 to 50 km offset). At higher values of Q the reflection amplitude clearly decreases at larger offsets. A number of studies indicate that values of Q for crystalline rocks in the upper crust below the surficial layers are generally in the 200 to 500 range for 10- to 30-Hz waves [e.g., *Braile*, 1977]; a Q value in the 100 to 200 range therefore seems reasonable, if not low. We can thus conclude that there is a net decrease of reflection amplitude with increasing offset. For Q=200, the SBS reflection amplitude at 18 km (30 degree incidence angle) is only 30% that of the zero-offset reflection; for Q=100 it is about 37% of the zero-offset amplitude.

The seismic reflection data over the SBS thus provide three constraints on the reflectivity: (1) the *P* wave reflection has a positive impedance contrast, (2) the reflection coefficient is relatively large, and (3) the *P* wave reflection amplitude decreases markedly for increasing incidence angles of up to about 30 degrees and perhaps beyond. Note that in the following AVO modeling we will be looking at first-order effects, that is, a positive or negative AVO response of about the same magnitude as the observed response, and not at the small variations of the AVO curve (which are likely local perturbations due to near-surface effects).

Without shear wave reflectivity measurements it is impossible to uniquely constrain the lithology by defining the density, Vp, and Vp/Vs changes across the SBS reflector, but the fluid model proposed for the SBS has some distinctive properties which can be tested with these data. The positive impedance contrast indicates that the SBS, if it is caused by a fluid-filled porous zone, must originate from the interface between two fluids residing within the pores or fractures with the denser, higher-velocity, fluid below the interface. The *P* wave velocity of a porous rock is a weighted average of the pore fluid and matrix velocities [*Wyllie et al.*, 1956, 1958] with a velocity increase at the fluid-fluid contact within the porous zone. Because fluids cannot support shear stresses, however, the shear wave velocity is largely insensitive to the type of pore fluid [e.g., *Ensley*, 1984; *Robertson and Pritchett*, 1985]. Two-fluid porous zones are thus characterized by an increase in the Vp/Vs ratio, or Poisson's ratio, across the fluid-fluid interface [*Ensley*, 1984]. The strength of the SBS reflection requires that there be a significant difference between the two pore fluids, so the Poisson ratio increase should not be a subtle effect in this case.

Modeling the observed AVO response demonstrates an inherent paradox with the fluid model: an increase in the Vp/Vs ratio across the reflector tends to produce a positive AVO trend

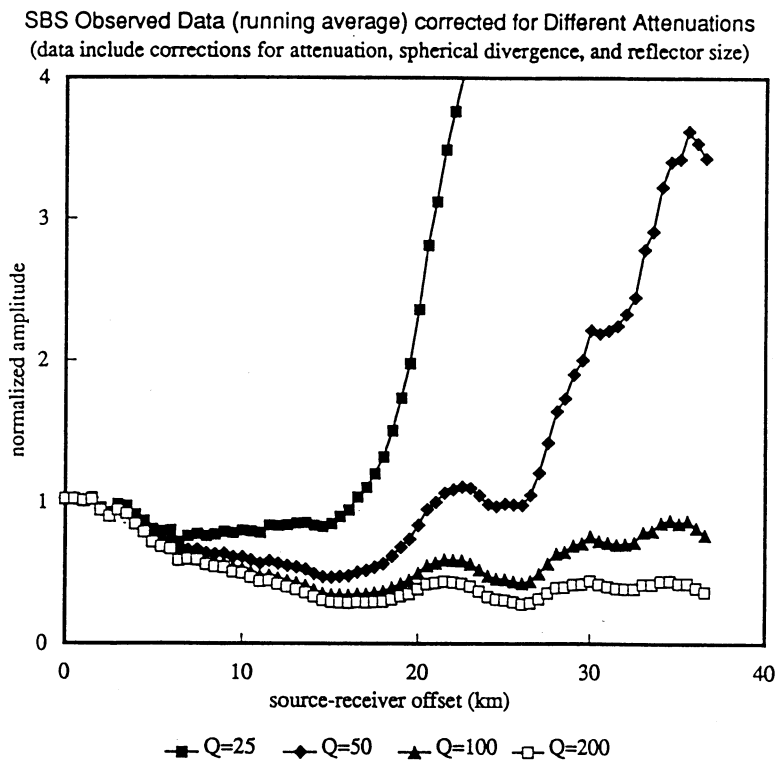

Fig. 12. SBS field data (running average over a 4-km offset range) corrected for spherical divergence, attenuation (four different values of Q), and reflector size. The residual AVO response shown here is due to the material properties of the reflector. Amplitudes between 25 and 40 km are probably noise levels (see Figure 5).

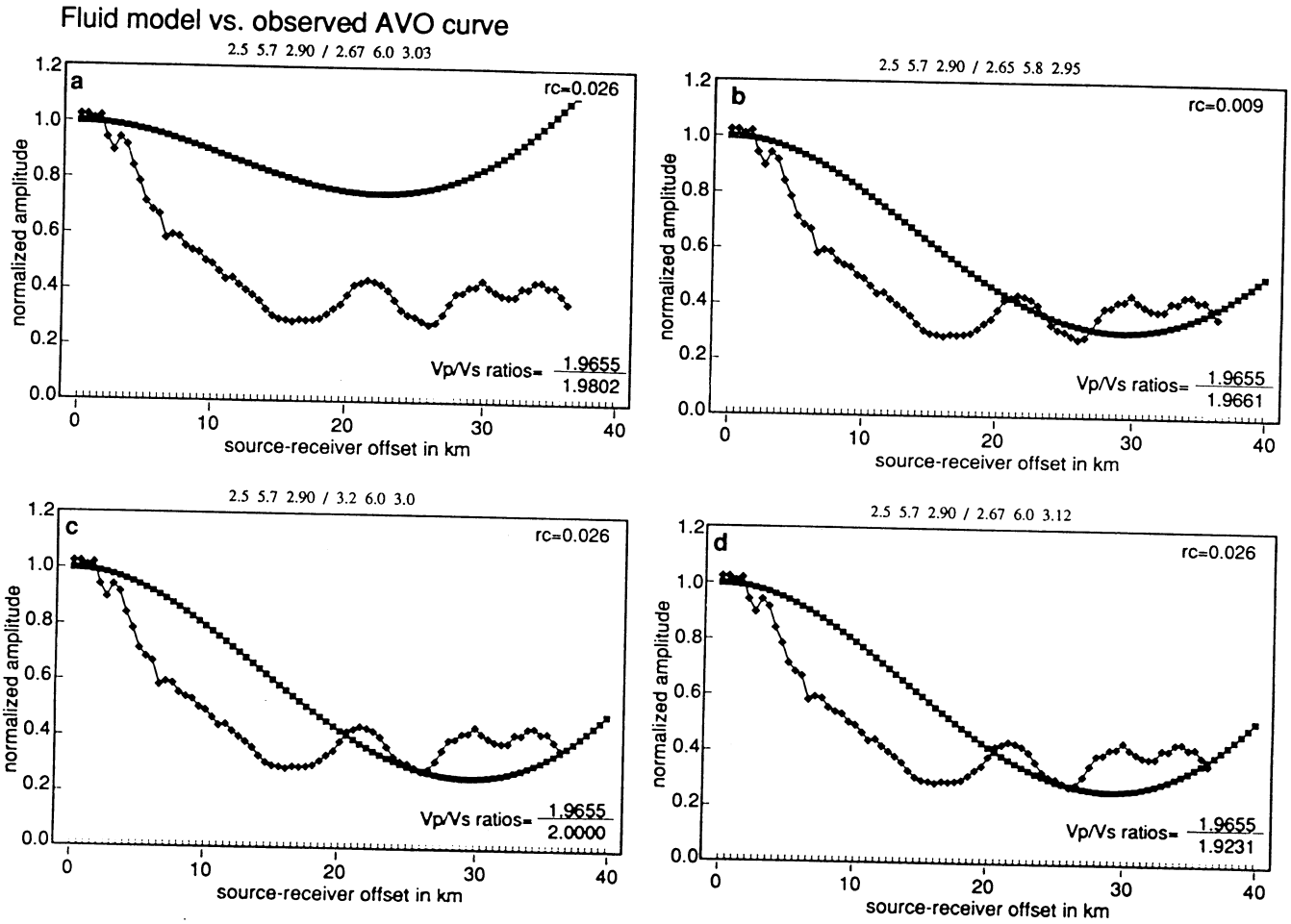

Fig. 13. Observed AVO response from the SBS, compared to the response for various fluid-filled porous zone models. Density, Vp, and Vs, respectively, are shown for both layers at the top of each graph; Vp/Vs ratios for both layers and the reflection coefficient (rc) are shown on the right. (*a*) Initial model with a moderate Vp, Vp/Vs, and density increase across the reflector. (*b*) The Vp and Vp/Vs increases across the reflector have been reduced to match the AVO response, but the reflection coefficient is now far too low to cause a bright reflection. (*c*) Same velocities as *a*, but an unreasonable (30%) density contrast is required to match the observed AVO response. (*d*) A decrease in the Vp/Vs ratio across the reflector allows for a variety of velocity and density increases to reproduce the AVO response and still have a significant reflection coefficient, but the model contradicts the fluid hypothesis.

(increasing amplitude at greater offsets) unless accompanied by either an extremely low reflection coefficient or an unreasonably large density increase. Using Zoeppritz's equations for the amplitude of the reflected wave at different incidence angles [*Aki and Richards*, 1980, pp. 149-150], we can test a fluid model with a reasonable increase in density, Vp, and Vp/Vs across the interface. Figure 13a, one of a large suite of similar models tested, shows that such a model does not reproduce the observed AVO response. As noted by previous workers [e.g., *Yu*, 1985; *Ostrander*, 1984], reflectors with a Vp/Vs increase tend to have a flat or positive AVO response. This problem can be circumvented by making the Vp and Vp/Vs increases very small (Figure 13*b*), but this in turn produces an extremely small reflection coefficient. Keeping the Vp/Vs increase small but using a substantial Vp contrast does not match the AVO response without using an unacceptably high (10% or greater) density increase (Figure 13*c*). Such a density increase is acceptable between differing lithologies but in the fluid model the density change must be accomplished by changing the density of the pore fluid, which presumably forms a small percentage (less than 20%) of the total rock mass.

A Vp/Vs decrease across the interface (Figure 13*d*) will match the observed AVO response with reasonable values for density, velocity, and reflection coefficient. This contradicts the fluid model unless the lower, denser liquid in the porous zone has a slower velocity to produce a Vp/Vs decrease across the interface; laboratory results do not preclude this (mercury has a slightly lower velocity than seawater), but for common materials the denser fluid has a faster velocity [*Birch*, 1942; *Carmichael*, 1982]. Furthermore, a velocity decrease and density increase would tend to work against each other to produce a relatively small reflection coefficient. Given these results, the simple two-fluid porous zone model appears implausible.

A mafic or ultramafic body, on the other hand, easily produces a negative AVO response of the proper magnitude because we are not constrained regarding the Vp/Vs ratio and because we can have relatively large increases in velocity and density across the interface. Figures 14*a*-14*c* show several models wherein the velocity and density contrasts are adjusted over a relatively wide range. The models match the magnitude of the observed AVO response, and the slopes of the model and observed curves are similar over much of their range. Given the variables involved, the models yield a remarkably good fit to

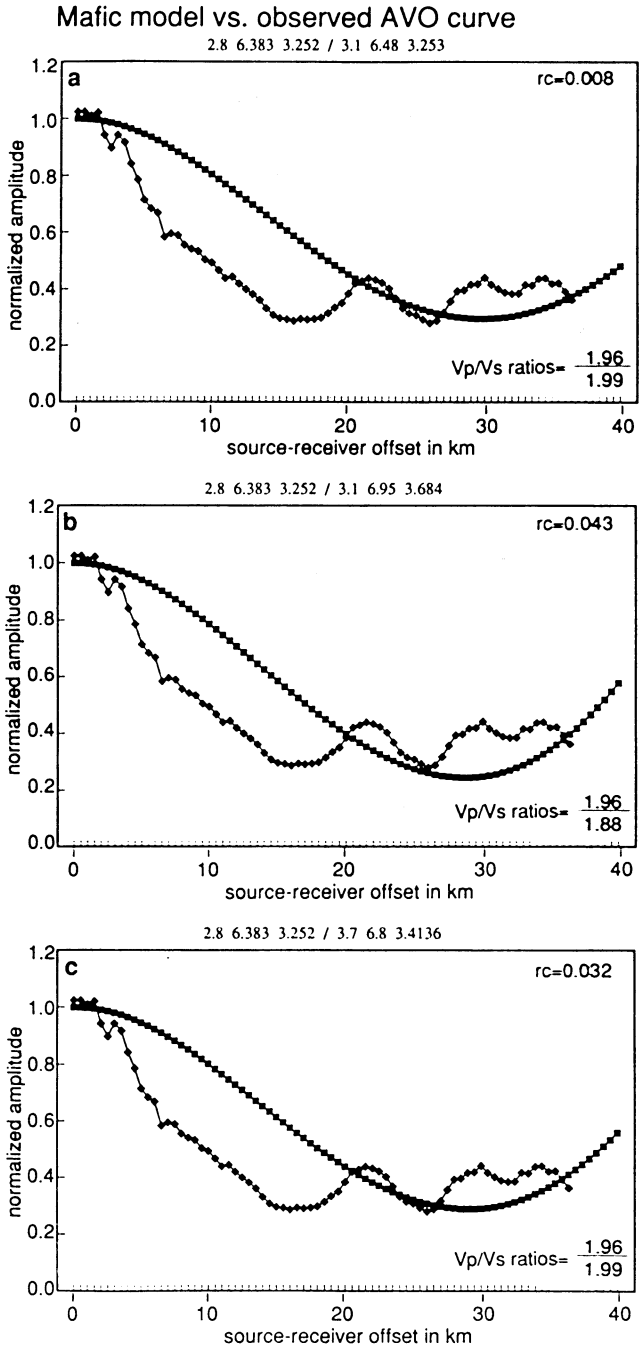

Fig. 14. Observed AVO response from the SBS compared to several mafic body models. Density, Vp, and Vs, respectively, are shown for both layers at the top of each graph; Vp/Vs ratios for both layers and the reflection coefficient (rc) are shown on the right. Note that there are a variety of density, velocity, and Vp/Vs contrasts which produce acceptable AVO responses. The wide lattitude in parameters possible for the mafic model make it easy to reproduce the observed AVO response and retain a sizeable reflection coefficient (0.3 to 0.5).

the data. We thus conclude that a wide range of mafic rocks such as basalt or gabbro could satisfy the AVO data. In addition, the mafic model allows for relatively large velocity and density changes to produce a reflection coefficient of 0.03 or greater (Figures 14*b* and 14*c*).

Discussion

The AVO analysis was successful in eliminating the fluid model only because the latter had unique properties to which the AVO response is especially sensitive. In fact, the analysis was useful because the reflection polarity at normal incidence is independent of the shear wave velocity contrast (no converted phases). The polarity test thus afforded an independent constraint, the *P* wave velocity increase, which was crucial to the analysis. An integral part of any AVO experiment should be a reflection polarity test.

Clearly, it would have been helpful to have independent constraints on the shear wave velocities by determining the shear wave reflection polarity and/or AVO response. The former is a much more difficult determination than the compressional wave polarity, particularly when working with reflectors so deep that shear waves are weak. The shear wave AVO response, particularly in *SH* (transverse) mode would likewise have been extremely useful. Alternatively, the use of converted phases (*P* to *SV*) could provide the shear wave velocity information. Unfortunately, no shear wave reflections from the SBS were strong enough for us to analyze effectively, and converted phases are also not obvious on the data.

Another piece of data which would have been extremely useful is the relative *P* and *S* wave reflection amplitudes at vertical incidence. The lack of reflections from below the SBS on shear wave data, as well as the relatively weak SBS reflection itself, prevented a quantitative analysis like that done by *Robertson and Pritchett* [1985]. Because the vertical reflections in each wave mode are independent of the other modes (no mode conversion), the *P* and *S* reflection coefficients independently measure the ratio of their respective velocity contrasts. This ratio would have been an important constraint in the modeling.

The experiment was successful in recording only a weak shear wave reflection from the SBS using vibrator sources. There are several potential causes of the weak *S* wave reflection, including vibrator coupling, near-surface attenuation, and shear wave splitting. We have not attempted to analyze the SBS data to isolate these effects and, indeed, it is probably impossible to separate them without further field studies. Though these early results indicate that an intensive shear wave effort is required (4 to 8 times the *P* wave effort, for example), further tests of shear wave vibrators for deep crustal work are warranted solely because the potential benefits are so high.

Conclusions

COCORP expanding spread profiles over the midcrustal Surrency Bright Spot (SBS) provide a well-constrained crustal velocity model which includes a relatively low-velocity deep crust. The uppermost layer corresponds with the 1.5-km-thick Atlantic Coastal Plain (ACP) sedimentary strata (Vp=2530 m/s; Vs=1510 m/s; Vp/Vs=1.67) below which is the crystalline upper crust between the ACP strata and the 16-km-deep SBS (Vp=6380 m/s; Vs=3250 m/s; Vp/Vs=1.96). The relatively low velocities in the lower crust (Vp=6020 m/s; Vs~3620 m/s) between the SBS and Moho is likely the result of underthrusting of relatively low-velocity upper crustal rocks (metasediments?) during the suturing of African crust (Florida) to North America. The reflection velocities are consistently slower than refraction velocities in the region, probably due in part to anisotropy, with horizontal energy traveling about 6% faster than the vertical energy.

Results of the reflectivity work over the Surrency Bright Spot (SBS) indicate that the SBS originates from an amphitheatre-shaped body about 2.2 km in diameter with the deep and flat portion to the southwest and that the SBS reflector is a high-

impedance body about 80 to 120 m in thickness. The latter result indicates that the reflection most likely originates from a mafic sill or ultramafic body in the midcrust and that the initial fluid hypothesis is untenable. Such a feature may have been emplaced either tectonically, during the Late Paleozoic suturing, or magmatically, most likely during the subsequent Mesozoic extension.

The results indicate that shear wave vibrators have the penetration capability for limited middle and lower crustal work but that a shear wave source effort 4 or more times that of the *P* wave effort, as measured by vibration time, is required. Other areas may be more conducive to shear wave work, and the potential rewards of shear wave information certainly make further tests desireable.

Acknowledgments. Funding for the data acquisition was provided by National Science Foundation grant EAR-8916129 to Cornell's Consortium for Continental Reflection Profiling (COCORP). Amoco Production Company generously donated equipment and substantial personnel time to the study. We thank John Myers and the technical and research staff of Amoco Production Company in particular for their efforts in the field. Personnel for the field crew were from Grant-Norpac under the direction of Ken Freeman. The experiment took place largely on the property of the Union Camp Corporation who kindly allowed us to freely roam their property. We are indebted to the Appling and Wayne County highway departments for allowing us to use the shear wave vibrators on the roads they maintain. Data processing was done primarily on the Cornell Theory Center's IBM 3090-600E computers at the Cornell National Supercomputer Facility, COCORP's SierraSeis seismic processing system, and the U.S. Geological Survey's Promax system. Steve Gallow, Kathleen Vargason, and Jane Axemathy provided technical assistance. The paper has benefited from discussions with Art Barnes, Sid Kaufman, Doug Nelson, and Jack Oliver at Cornell and Dan Johnson, Richard Heiser, and John Myers at Amoco. Institute for the Study of the Continents (INSTOC) contribution 184.

REFERENCES

Aki, K., and P.G. Richards, *Quantitative Seismology, Theory and Methods*, vol. 1, 555 pp., W. H. Freeman, New York, 1980.

Al-Chalabi, M., Series approximation in velocity and traveltime computations, *Geophys. Prospect.*, *21*, 783-795, 1973.

Backus, M., and R.L. Chen, Flat-spot exploration, *Geophys. Prospect.*, *23*, 533-577, 1975.

Barnes, A.E., and T.J. Reston, Analysis and interpretation of midcrustal bright spots within the Alleghanian suture of southeast Georgia, *Geophys. J. Int.*, *108*, 683-691, 1992.

Birch, F. (Ed.), Handbook of Physical Constants, *Spec. Pap. Geol. Soc. Am.*, *36*, 325 pp., 1942.

Braile, L.W., Interpretation of crustal velocity gradients and Q structure using amplitude-corrected seismic refraction profiles, in *The Earth's Crust, Geophys. Monogr. Ser.*, vol. 20, edited by J.G. Heacock, pp. 427-439, AGU, Washington, D.C., 1977.

Brown, L.D., D. Wille, L. Zheng, B. deVoogd, J. Mayer, T. Hearn, W. Sanford, C. Caruso, T.-F. Zhu, K.D. Nelson, C. Potter, E. Hauser, S. Klemperer, S. Kaufman, and J. Oliver, COCORP: New perspectives on the deep crust, *Geophys. J.*, *89*, 47-54, 1987.

Carmichael, R.S., (ed.), *Handbook of Physical Properties of Rocks*, vol. 2, 345 pp., CRC Press, Boca Raton, Fl., 1982.

Chowns, T.M., and C.T. Williams, Pre-Cretaceous rocks beneath the Georgia coastal plain - regional implications, in Studies Related to the Charleston, South Carolina Earthquake of 1886 - Tectonics and Seismicity, edited by G.S. Gohn, *U.S. Geol. Surv. Prof. Pap.*, *1313*, L1-L42, 1983.

Christensen, N. I., Reflectivity and seismic properties of the deep continental crust, *J. Geophys. Res.*, *94*, 17,793-17,804, 1989.

Dobrin, M.B., *Introduction to Geophysical Prospecting*, 3rd ed., 630 pp., McGraw-Hill, New York, 1976.

Ensley, R.A., Comparison of P- and S-wave seismic data: A new method for detecting gas reservoirs, *Geophysics*, *49*, 1420-1431, 1984.

Fyfe, W.S., Fluids in deep continental crust, in *Reflection Seismology: The Continental Crust, Geodyn. Ser.*, vol. 14, edited by M. Barazangi and L. Brown, pp. 33-40, AGU, Washington, D.C., 1986.

Madabhushi, S., P. Talwani, H. Benz, J. Luetgert, W. Mooney, and E. Criley, Shallow crustal structure beneath the South Carolina Coastal Plain, *Eos Trans. AGU*, *72*, Fall Meeting Suppl., 428, 1991.

McBride, J.H., and K.D. Nelson, Integration of COCORP deep reflection and magnetic anomaly analysis in the southeastern United States: Implications for the origin of the Brunswick and East Coast magnetic anomalies, *Geol. Soc. Am. Bull.*, *100*, 436-445, 1988.

Mondary, J.F., T.L. Pratt, and L.D. Brown, A three-dimensional look at the Surrency Bright Spot beneath southeastern Georgia, Paper presented at 61st Annual Meeting, Soc. of Explor. Geophys., Houston, Tex., November 10-14, 1991.

Mondary, J.F., T.L. Pratt, and L.D. Brown, Three-dimensional geometry of the midcrustal Surrency Bright Spot beneath southeastern Georgia, *Geophysics*, in press, 1993.

Nelson, K.D., J.A. Arnow, J.H. McBride, J.H. Willemin, J. Huang, L. Zheng, J.E. Oliver, L.D. Brown, and S. Kaufman, New COCORP profiling in the southeastern United States, Part I: Late Paleozoic suture and Mesozoic rift basin, *Geology*, *13*, 714-718, 1985*a*.

Nelson, K.D., J.H. McBride, J.A. Arnow, J.E. Oliver, L.D. Brown, and S. Kaufman, New COCORP profiling in the southeastern United States, Part II: Brunswick and East Coast magnetic anomalies, opening of the north-central Atlantic Ocean, *Geology*, *13*, 714-718, 1985*b*.

Ostrander, W.J., Plane-wave reflection coefficients for gas sands at nonnormal angles of incidence, *Geophysics*, *49*, 1637-1648, 1984.

Pratt, T.L., E.C. Hauser, T.M. Hearn, and T.J. Reston, Reflection polarity of the midcrustal Surrency Bright Spot beneath southeastern Georgia: Testing the fluid hypothesis, *J. Geophys. Res.*, *96*, 10,145-10,158, 1991.

Robertson, J.D., and W.C. Pritchett, Direct hydrocarbon detection using comparative P-wave and S-wave seismic sections, *Geophysics*, *50*, 383-393, 1985.

Robinson, E.A., and Treitel, S., *Geophysical Signal Analysis*, 466 pp., Prentice-Hall, Englewood Cliffs, N.J., 1980.

Taner, M.T., and F. Koehler, Velocity spectra-digital computer derivation and applications of velocity functions, *Geophysics*, *34*, 859-881, 1969.

Taner, M.T., and F. Koehler, Surface consistent corrections, *Geophysics*, *46*, 17-22, 1981.

Taylor, S.R., Geophysical framework of the Appalachians and adjacent Grenville Province, in Geophysical Framework of the Continental United States, edited by L.C. Pakiser and W.D. Mooney, *Mem. Geol. Soc. Am.*, *172*, 317-348, 1989.

Wille, D.M., The COCORP Surrency bright spot: Fluid in the deep crust?, M.S. thesis, 46 pp., Cornell Univ., Ithaca, N.Y., 1987.

Wyllie, M.R.J., A.R. Gregory, and G.H.F. Gardner, Elastic wave velocities in heterogeneous and porous media, *Geophysics*, *21*, 41-70, 1956.

Wyllie, M.R.J., A.R. Gregory, and G.H.F. Gardner, An experimental investigation of factors affecting elastic wave velocities in porous media, *Geophysics*, *23*, 459-493, 1958.

Yu, G., Offset-amplitude variation and controlled-amplitude processing, *Geophysics*, *50*, 2697-2708, 1985.

L. D. Brown, Institute for the Study of the Continents (INSTOC), Cornell University, Ithaca, NY 14853.

N. I. Christensen, Department of Earth and Atmospheric Sciences, Purdue University, West Lafayette, IN 47907.

S. H. Danbom, Conoco, Incorporated, P.O. Box 1267, Ponca City, OK 74603.

J. F. Mondary, Amoco Production Company, P.O. Box 3092, Houston, TX 77253.

T. L. Pratt, Branch of Earthquake and Landslide Hazards, U. S. Geological Survey, Mail Stop 966, Denver Federal Center, Denver, CO 80225.

(Received June 22, 1992;
revised June 24, 1993;
accepted June 30, 1993.)